11th International Symposium on Turbulence and Shear Flow Phenomena (TSFP11)
Southampton, UK, July 30 to August 2, 2019

PROPER ORTHOGONAL DECOMPOSITION OF A TURBULENT JET INTERACTING WITH A FREE SURFACE

Vesselina Roussinova

Department of Mechanical, Automotive and Materials Engineering

University of Windsor
401 Sunset Ave.
Windsor, ON, Canada

Email: vtr@uwindsor.ca

Ram Balachandar

Department of Civil and Environmental Engineering

University of Windsor
401 Sunset Ave
Windsor, ON, Canada

Email: rambala@uwindsor.ca

ABSTRACT

This paper investigates the large-scale coherent structures of a turbulent jet interacting with a free surface using high-resolution planar particle image velocimetry (PIV) and proper orthogonal decomposition (POD). The PIV measurements reveal important information about the complex interactions between the jet and the deforming free surface. The velocity characteristics and vorticity are studied in the horizontal planes just beneath the free surface in the interaction region of the jet at $30 < x/d < 62$. Here, d is the nozzle diameter. The jet exit velocity was kept at 2.8 m/s, corresponding to a jet Reynolds number of 28,000. The jet was submerged 5d below the free surface. To investigate the jet structures interacting with the free surface, the present surface jet analysis is complemented with the analysis of the reference case of the deep (free) jet at similar flow conditions. This study further explores the characteristics of the large- scale structures by decomposing the fluctuating velocity and vorticity fields using proper orthogonal decomposition (POD). The snapshot method decomposes velocity field to a set of spatial modes and time varying coefficients. The snapshot POD velocity and vorticity modes were ranked according to the size of the eigenvalues. While low-rank modes represent the most energetic and least isotropic structures in the flow field, the intermediate and high ranking modes tend to be more isotropic and are associated with random small-scale turbulence. The resulting low-rank POD modes in various horizontal and vertical center planes were compared with the undisturbed free jet at similar flow conditions. Despite the truncation of the turbulent kinetic energy due to the finite size of the PIV field-of-view (FOV), we were able to observe some differences for the near surface jet case which could be related to the confinement effects of the free surface.

INTRODUCTION

Turbulent jets have significant fundamental and practical importance and they are extensively used in enhancing and controlling mixing, heating and combustion processes. In many practical situations, the jet flows can be confined either by the free surface or by the solid wall. Confined jets differ from the free (unconfined) jets in many ways. For instance, the presence of a free surface or a solid wall constrains the entrainment of ambient fluid into the jet and diminishes the turbulence fluctuations normal to the free surface. This anisotropy leads to significant increase of the jet-spreading rate in the plane parallel to the free surface affecting the turbulence transport near the boundaries. Though a similar behaviour has been noted in wall jets, the surface jets differ due to the non-zero mean velocity observed at the free surface. While the mean velocity and statistical turbulence properties of the free jets are well documented (e.g., Rajaratnam, 1976, Fischer et al., 1979; Wood et al., 1993, Shinneeb et al., 2008, Tandalam et al., 2010, Rahman et al., 2018), very little is known about the behaviour of turbulent flows adjacent to a free surface.

The present study is a continuation of a previous work on near-surface turbulent jet (Tian et al., 2011). Previous results revealed that the behavior of the surface jet was very similar to that of the free jet before it interacts with the free surface. Following the free surface interaction, the velocity component normal to the free surface was diminished and those parallel to the free surface were enhanced in the region near the free surface. In the horizontal plane near the free surface, the spreading of the surface jet was significantly greater than that of the free jet. It was found that the mean lateral flow tends to be outward everywhere for the surface jet, while the opposite trend occurs in the free jet. The magnitude of Reynolds shear stress in the vertical central plane of the surface jet was smaller than that noticed in the free jet. An increase in the normal component of vorticity was also observed in the horizontal planes near the free surface. The impediment of the jet shear layer by the free surface is expected to affect the entertainment and large scale structures. The objective of this paper is to provide more details for the turbulence structures of the surface jet by utilizing the vorticity and proper orthogonal decomposition (POD).

METODOLOGY

Proper Otrhogonal Decmosition (POD)

Proper orthogonal decomposition (POD) offers a way to decompose the flow structures and group the energetic flow structures that are coherent. This technique is often used as a tool to examine the structures spatial extent and to study their contribution to the turbulent transport. To identify the dominant flow structures in the surface jet, the snapshot Proper Orthogonal Decomposition (POD) is performed on large ensemble of flow fields (see e.g. Lumley, 1967; Sirovich, 1987). Since POD is based on energy considerations, if large energetic flow structures systematically appear they will be captured by only few low-rank POD modes. The objective here is to examine the structure of the low-rank POD modes in the case of surface jet and compare them with the unperturbed case of an axisymmetric free turbulent jet at the same flow condition. In doing so, the effect of the free surface perturbation on the subsurface turbulence and coherent structures will be revealed. In the current study, we use proper orthogonal decomposition (POD) to separate the coherent and incoherent turbulent kinetic energy contributions to the total turbulent kinetic energy, in addition to spatially describing the patterns contributing most significantly to the total turbulent kinetic energy. It is often thought that the increased mixing observed in the turbulent jets is reflected by the increase of the magnitude of the turbulent kinetic energy. One the other hand, mixing might be significantly affected by the free surface by actively modifying the large scales structures in the surface jet without a noticeable change to the distributions of the mean velocity or turbulence intensity as noted by Wiltse and Glezer (1998). The structurally significant POD modes of the surface jet analysed in the interaction region and their effect is investigated by comparison with the reference free jet case.

For the snapshot method (spatial POD), an ensemble of spatio-temporal array is defined by

$$\mathbf{U} = \left\{\mathbf{U}_{\mathbf{i}}\right\}_{i=1}^{M} = \begin{bmatrix} u_{11} & u_{12} & \cdots & u_{1M} \\ u_{21} & u_{22} & \cdots & u_{2M} \\ & \vdots & & \\ u_{N1} & u_{N2} & \cdots & u_{NM} \end{bmatrix}, \tag{1}$$

where $\mathbf{U} = [\boldsymbol{u_1}, \boldsymbol{u_2}, \ldots \boldsymbol{u_N}]^T$ consists of fluctuating velocity vectors for a total of N snapshots. In the method of snapshots, the $M \times M$ spatial autocovariance matrix is constructed such that

$$\boldsymbol{R} = \mathbf{U}^{\boldsymbol{T}}\mathbf{U}\,. \tag{2}$$

In Eq. 2, the variables used for the POD analysis will be the two planar velocity components, u and v available in the vertical center plane and u and w available in the horizontal planes. Solving an eigen value problem given by

$$\boldsymbol{R\phi} = \boldsymbol{\lambda\phi} \tag{3}$$

yields the eigenvalues, $\boldsymbol{\lambda}$ and eigenvectors, $\boldsymbol{\phi}$. The eigenvalues are further arranged, and the spatial POD modes are computed. The k-th spatial POD mode is given by

$$\Phi_k(x) = \frac{\boldsymbol{V\phi_k(t)}}{\|\boldsymbol{V\phi_k(t)}\|}\,. \tag{4}$$

The expansion coefficients for each snapshot of the k-th mode are defined as

$$a_k(t) = \boldsymbol{\phi_k(t)}\|\boldsymbol{V\phi_k(t)}\|\,. \tag{5}$$

This form of POD decomposes the spatial correlation array and leads to spatially orthogonal modes that are modulated in time by expansion (time) coefficients with random time dependence. The time coefficients, $a_k(t)$, can be plotted against each other on the phase portrait to identify the phase relation between them. If the phase portrait forms a circular ring as reported by Weightman et al. (2018) then the two modes formed a modal pair describing periodic flow phenomena. This approach was used to investigate the shear layer of the supersonic impinging jet and the flow past a bluff body (Tang et al., 2015 and Tang et al., 2018) where in both cases it was found that the kinetic energy is concentrated in a few spatial POD modes with clearly defined modal pairs determined from the phase portrait of the corresponding time coefficients. In many turbulent flows, due to their complex structure deviations from this perfectly periodic mode pairs occur. This results in snapshots laying randomly off the annular distribution on the phase portrait. Random distributions of time coefficients were observed for the case of a turbulent jet in cross flow by Meyer et al., (2007) as well as in turbulent boundary layer flow studied by Wu (2014). It appears that the circular distribution of the time coefficients (a_1, a_2) is most likely to indicate a cyclic variation of POD modes, which is exactly what is expected if two POD modes describe different phases of a regular periodic process. This also conforms to the definition of a coherent structure which appear regularly with a fixed frequency. Often the information for the phase obtained from experiments is contaminated and different approaches are described in the literature to select only FOVs that are clean or statistically significant based on certain criteria. For example, Meyer et al., (2007) eliminates all FOVs that does not satisfy two criteria: i) the sum of squares $a_1^2 + a_2^2$ is closer to the mean value and ii) $|a_1| \approx |a_2|$. Only FOVs matching these criteria are included in the reconstruction. We have applied similar approach to organize the time coefficients of PIV snapshots of the surface jet reconstruction using the first two POD modes.

EXPERIMENTS

The experiments were conducted in a jet facility 2 m long, 1 m wide and 0.7 m deep. A circular cross-section nozzle was mounted on the side wall of the tank made of 2 cm thick aluminum plate. The center of the nozzle was located 0.3 m above the bottom of the tank, and 0.5 m away from both side walls of the tank. The nozzle opening was 10 mm in diameter and it was mounted flush with the inside wall of the tank. Jet discharge was provided by an overhead reservoir with a constant supply head of 2 m. The water level in the jet tank was controlled by an adjustable downstream sharp-crested plate. The flow from the overhead reservoir was controlled by a valve and was calibrated with a flowmeter to deliver a constant velocity of 2.8 m/s at the jet exit. The surface jet was produced by positioning of the jet exit near the free surface at a submergence ratio, $H/D = 5$. Here, H denotes the vertical depth of the water measured from the free surface to the center of the jet. The submergence was chosen and optimized based on minimal effect of the surface waves on the quality of the velocity measurements. The Reynolds number based on the jet diameter (d) and exit velocity (U_j) was $Re = U_j d/\nu = 28{,}000$.

The velocity field was measured using a planar Particle Image Velocimetry (PIV) system. The water in the tank was seeded with 12 µm silver-coated hollow glass spheres with a density of 1130 kg/m^3. The seed particles were illuminated over a predefined field-of-view (FOV) with overlapping laser light sheet generated by a pair of Nd:YAG lasers with a maximum power of 50 mJ per pulse at a wavelength of 523 nm and pulse width of 10 ns. The laser sheet was generated by a combination of spherical and cylindrical lenses with focal length of 500 mm and a -15 mm, respectively. The thickness of the light sheet in the FOV was ~ 1 mm. A TSI Powerview Plus 4MP CCD camera with a resolution of 2048 × 2048 pixels was employed to record pairs of time delayed images of the particles. The image acquisition was performed with the software Insight 3G by TSI Inc. The pair of images was first interrogated with a window of 64 × 64 pixels using an FFT-based cross-correlation technique between the two successive images. The particle displacements from the previous coarse grid interrogation were reanalyzed with smaller 32 × 32 pixels interrogation window to improve the resolution and accuracy of the velocity field. At every stage, the interrogation areas were overlapped by 50%. The interrogation process yielded a final interrogation area of 16 × 16 pixels with a total of 127 × 127 vectors.

Following the correlation analysis, the invalid vectors were rejected by using the cellular neural network method with a variable threshold technique proposed by Shinneeb et al., (2004). On average, the percentage of the valid vectors was high enough (> 94%) and all rejected vectors were replaced by vectors calculated by using Gaussian-weighted mean interpolation. The PIV data were further low-pass filtered with a narrow Gaussian kernel with a width equal to two grid units ($2\Delta x$) to remove noise due to the frequencies larger than the sampling frequency of the interrogation. The estimated uncertainty in the mean velocity, Reynolds stresses and vorticity were ± 2%, ± 5% and ± 7%.

Figure 1a shows the iso-contours of mean streamwise velocity in the surface jet. The contours were plotted for 30 < x/d < 62 where the jet interacts and attaches to the free surface. As the entrainment of ambient fluid is constrained by the free

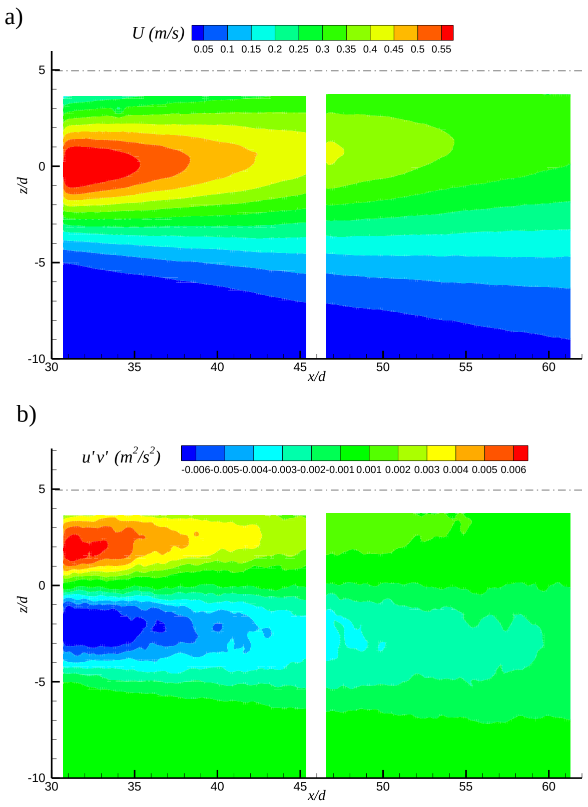

Figure 1. Iso-contours of mean velocity (a) and Reynolds shear stress, $\overline{u'w'}$, (b) of surface jet at vertical (x - z) central plane.

surface the maximum velocity of the jet is shifted slightly upwards to accommodate the development of accelerating surface current. The Reynolds shear stress depicted in Figure 1b, also show asymmetry in the distribution of the upper and lower shear layers. The $\overline{u'v'}$ in the upper shear layer is attenuated by the interaction with the free surface and it is close to zero for x/d > 50. On the other hand, the lower shear layer is unimpeded accommodating mixing and entrainment.

VORTICITY

The vorticity field is calculated from the instantaneous velocity gradients using the Richardson extrapolation technique. Figures 2a and 2b show average vorticity profiles of both surface and free jets in the horizontal plane (x - y) at two streamwise locations (x/d = 38 and 54). Normal vorticity $\langle\omega_z\rangle$ is examined not only in the central plane of the jet (z/d = 0) but also at different offset distances z/d = -3 and +3. At x/d = 38, a similar magnitude of vorticity is obtained for both free and surface jets at z/d = 0. Higher magnitude of vorticity is obtained at y/d = ±2 where the shear layers are well developed. In Figure 2a, due to

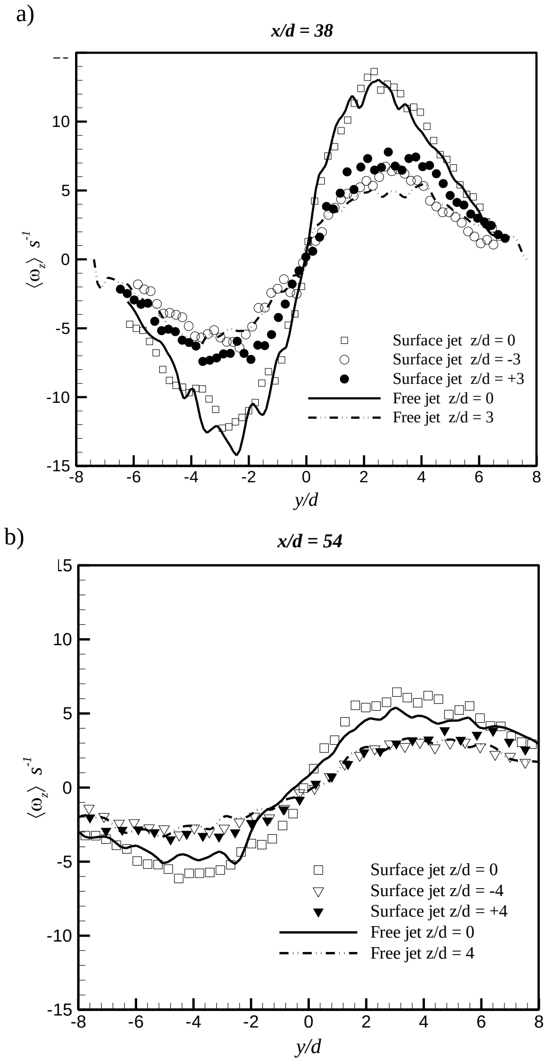

Figure 2. Surface and free jet vorticity profiles $\langle\omega_z\rangle$ in horizontal (x - y) plane (a) x/d =38 and (b) x/d =54.

the deeper submergence of the jet (h/d = 5) no significant change of $\langle\omega_z\rangle$ is noted at planes z/d = +3 and -3 where the vorticity magnitude is reduced, and the axisymmetric behavior of the jet is still intact. At this streamwise location, the vorticity of the surface jet resembles the vorticity of the free jet. As the surface jet travels further downstream, the vorticity magnitude reduces even more. At x/d = 54, the profiles of the vorticity of the surface jet and free jet at z/d = 0 are similar. The surface jet vorticity near the free surface at z/d = ±4 is further reduced as shown in Figure 2b. At this streamwise location no significant differences of $\langle\omega_z\rangle$ are noted between the surface jet and free jet implying that the changes in the shear layers in horizontal planes is not influenced by the free surface.

In Figure 3 distributions of mean spanwise vorticity is examined at x/d = 38 and 54 for surface and free jets. Near the free surface, the spanwise vorticity of the surface jet is attenuated in both streamwise locations indicating modification of the

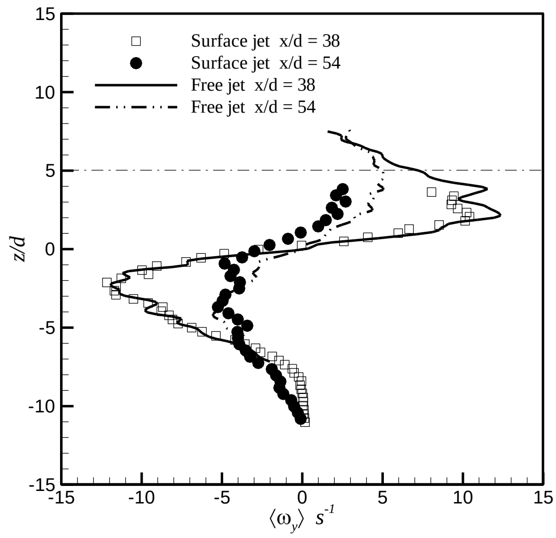

Figure 3. Surface and free jet vorticity profiles $\langle\omega_y\rangle$ in (x - z) plane (a) x/d =38 and (b) x/d =54. The dash-dot line denotes the free surface.

upper shear layer. Finite values of positive vorticity at the free surface at both streamwise locations suggest strong turbulence anisotropy and possible interactions of the local vorticity with its "image" above the free surface as observed by Walker (1997). Below the jet centerline $\langle\omega_y\rangle$ profiles are undisturbed and matching with the free jet profiles.

POD MODES

The asymmetry in the jet entrainment and the free surface anisotropy is further examined by calculating the POD modes in horizontal and vertical planes passing trough the jet centreline.

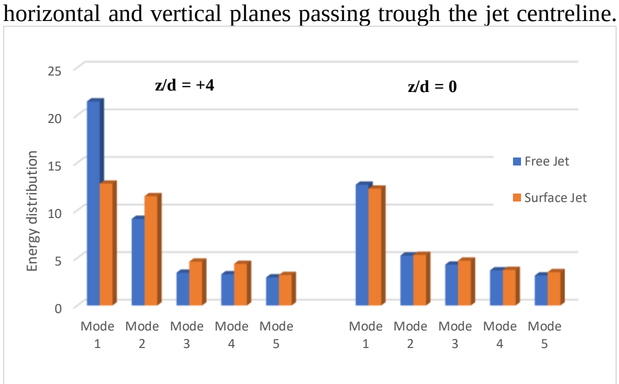

Figure 4. Fractional energy contributions of the first five POD modes in horizontal planes at z/d = +4 and 0 (central plane).

In Figure 4, the fractional energy contribution of the first five modes of the velocity POD decomposition were compared for the free and surface jets at 45 < x/D < 62. As expected the first two velocity modes in the near surface horizontal plane (z/d = +4) carry most of the energy of the large-scale structures. In the jet central horizontal plane, the modes in the velocity-POD contain similar energy contribution for both jets. The change in the energy content of the velocity-POD modes reflect the modification of the jet structure near the free surface. To check for the convergence, the eigenvalues of the velocity and vorticity POD decompositions are examined as a function of the number of the FOVs. To reach convergence for the velocity POD it was found that the number of the FOVs must be larger than 1500. For the vorticity POD decomposition, the convergence was considerably slower which increases the ensemble size and requires more than 2000 FOV's. The enstrophy content in the first two vorticity POD modes was significantly larger than others, which indicates that the first two vorticity POD modes embody the largest scales of the flow. In addition, although the energy contained in specific modes are very different between the free and the surface jet in most horizontal planes, it is very

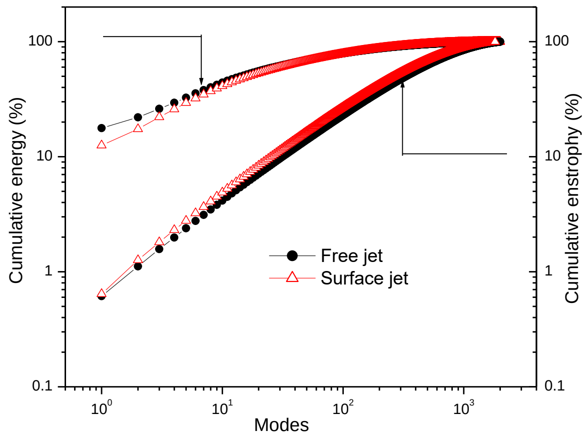

Figure 5. Cumulative energy and enstrophy calculated for free and surface jets in central vertical plane (x - z).

similar at the central vertical plane (y/d = 0) for all vorticity modes as shown in Figure 5.

The shape of the POD modes is examined and compared with reference case of the free axisymmetric jet in attempt to reveal some differences in turbulence structures. In Figure 6, the shape of the first four POD modes are shown in the center plane of both free jet and surface jet. The contours of each mode defined as $\phi_i = \sqrt{\phi_{u'}^2 + \phi_{v'}^2}$ are depicted for 30 < x/d < 45. Very similar shapes of the most energetic structures are observed in the horizontal plane for free and surface jets. Some differences are noted only in the higher rank Mode 4, containing only 3.6 % of the total TKE. This suggest that in the horizontal center plane the most energetic structures of surface jet are similar in shape to the structures of the free jet. It appears that in this plane, the effect of the free surface is only visible in the change of the shape of higher POD modes. It is conjectured that the effect of the free surface is felt in the jet central plane through modulation of the small-scale structures only. The shapes of the POD modes in the vertical central plane of the surface jet show significant changes indicating asymmetry due to the confinement of the free surface. It is interesting to note that the shape of the first vertical POD mode of surface jet resembles half of the free jet, with almost undisturbed lower half. The shapes of the velocity POD modes in the vertical plane resemble various stages of jet free surface interaction. It is also noted that the shapes of the even modes 2 and 4 are more affected than their odd counterpart most likely due to the symmetry of the problem. The shape of the vorticity POD modes was also investigated since previous study observed reduction of the enstrophy near the free surface (Bernal and Scherer, 1997). In the vertical central plane, the effect of the existing surface current is resulting in breaking the jet structure

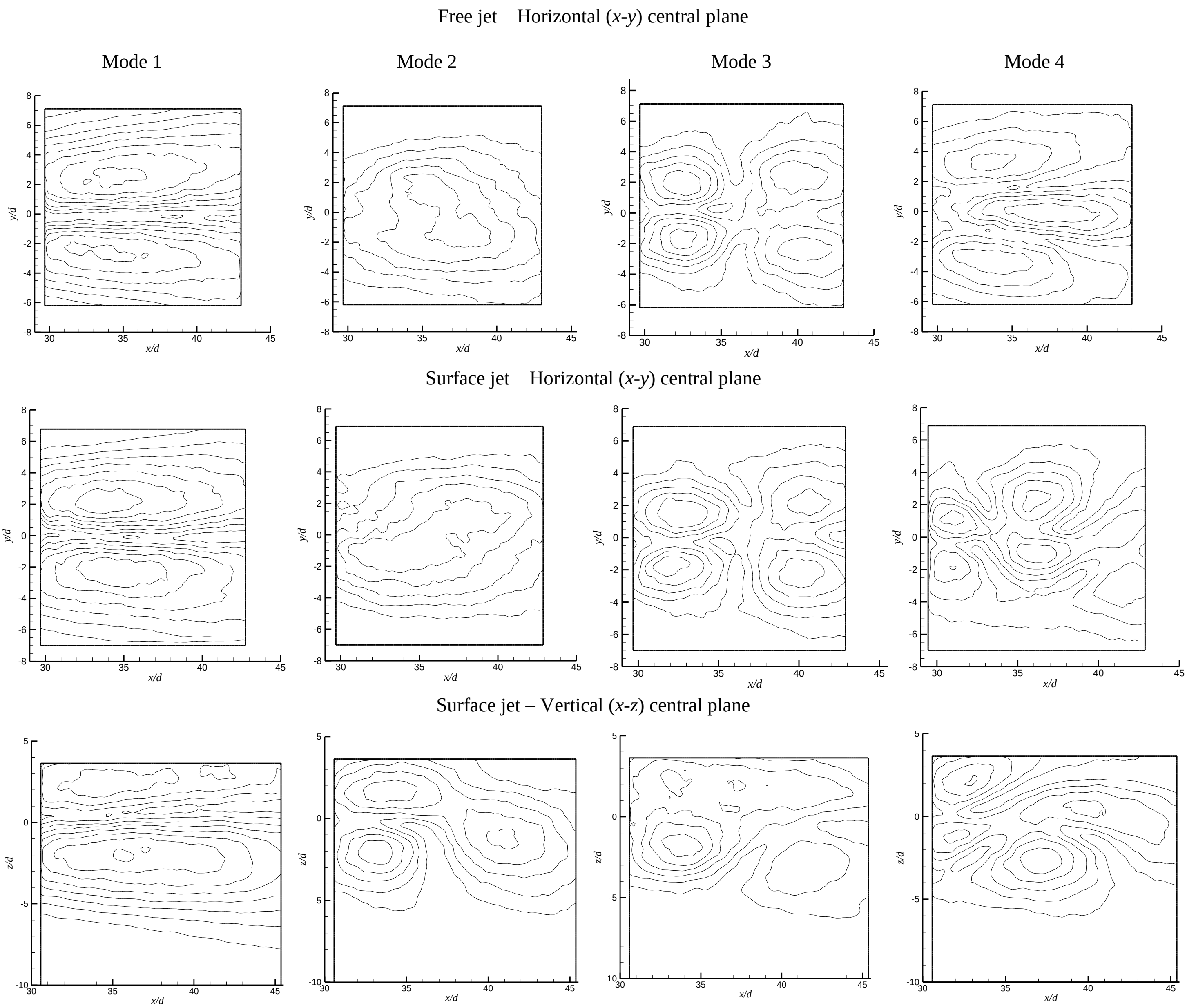

Figure 6. Four most energetic POD mode shapes defined as $\boldsymbol{\phi_i} = \sqrt{\boldsymbol{\phi^2_{u',i}} + \boldsymbol{\phi^2_{v',i}}}$. Comparison of free axisymmetric jet at horizontal plane. Contours varied from 0.5 to 2.5 with 0.5 division.

associated with vortex reconnection and stretching. The complete physical mechanism is still under investigation.

CONCLUSIONS

The characteristics of a round turbulent surface jet with a submergence ratio of *H/d* = 5 was investigated using PIV technique. The vorticity magnitude in horizontal planes farther from the jet central plane is reduced. No significant change of $\langle \omega_z \rangle$ is noted at planes *z/d* = -3 and +3 where the vorticity magnitude is reduced, and the axisymmetric behavior of the jet is still intact. Reduction of the vorticity component $\langle \omega_y \rangle$ for a surface jet is noted near the free surface at *x/d* = 54. The proper orthogonal decomposition (POD) technique was applied to the PIV data. Results show that the number of modes needed to capture 50% of the turbulent kinetic energy (TKE) is slightly more in the case of surface jet. It is also noticed that in the vertical central plane, similar number of vorticity POD modes are needed to capture 50% of the enstrophy for both free and surface jets. The shape of the POD vorticity modes (not shown in this paper) in the vertical plane were calculated and they reveal presence of predominantly small-scale structures in the near surface region.

REFERENCES

Rahman M. S., Tay G. F. K., Essel E. E., Tachie M., (2018),"Effects of offset height on the turbulent characteristics of a surface attaching jet", Int. J. of Heat Fluid Flow, Vol. 71, pp. 305-321.

Tang S.L., Djenidi L, Antonia R. A., Zhou Y., (2015), Comparison between velocity- and vorticity-based POD methods in a turbulent wake. Exp Fluids 56(8):169.

Tang S.L., Djenidi L, Antonia R. A., Zhou Y., (2018), “Secondary vortex street in the intermediate wake of a circular cylinder“, Vol. 59, 119. https://doi.org/10.1007/s00348-018-2577-1.

Tian, J., Roussinova, V., and Balachandar, R., (2012), “Characteristics of a jet in the vicinity of a free surface,” Journal o f Fluids Engineering, Vol. 134, pp. 1-12.

Rajaratnam, N. (1976), Turbulent Jets, Elsevier Scientific Publishing Company, Amsterdam.

Fischer, H. B., List, E. J., Koh, R. C. Y., Imberger, J. and Brooks, N. H. (1979). “Mixing in Inland and Coastal Waters”. New York: Academic.

Wood I. R. (1993) “Asymptotic solutions and behaviour of outfall flumes” J. Hydr. Eng. ASCE, 119: .555–580.

Shinneeb, A.M., Bugg, J.D. and Balachandar, R. (2008), Analysis of coherent structures in the far-field region of an axisymmetric free jet identified using particle image velocimetry and proper orthogonal decomposition, J. Fluids Eng., v.130, is. 1, pp. 21-29.

Tandalam A., Balachandar R. and Barron R. (2010) “Reynolds Number Effects on the Near-Exit Region of Turbulent Jets”. J. Hydr. Engrg. **136**: (9), 633-641.

Lumley, J. L. (1967), The structure of inhomogeneous turbulent flows. In Atmospheric Turbulence and Radio Wave Propagation (ed. A. M. Yaglom & V. I. Tatarsky), pp. 166-178. Nauka, Moscow

Sirovich, L. (1987), Turbulence and the dynamics of coherent structures. Part I: Coherent structures, Quarterly of Applied Math., v45, n3, pp. 561-571.

Wiltse, J. M. and Glezer A., “Direct excitation of small-scale motions in free shear flows,” Phys. Fluids **10**, 2026 (1998)

Meyer, K., Pedersen, J., and Özcan, O., (2007) “A turbulent jet in crossflow analysed with proper orthogonal decomposition“. Journal of Fluid Mechanics, (2007) 583, 199-227. doi:10.1017/S0022112007006143

Wu Y, (2014) “A study of energetic large-scale structures in turbulent boundary layer“ Phys. Fluids 26, 045113; https://doi.org/10.1063/1.4873199

Weightman, J.L., Amili, O., Honnery, D., Julio Soria J., and Edgington-Mitchell D., (2018), “Signatures of shear-layer unsteadiness in proper orthogonal decomposition”, Exp Fluids 59: 180. https://doi.org/10.1007/s00348-018-2639-4